Multi-segmental Spine Image Registration Supporting Image-guided Interventions of Spinal Metastases

Georg Hille[a,*], Sylvia Saalfeld[a], Steffen Serowy[b], Klaus Tönnies[a]

[a] *Department of Simulation and Graphics, University of Magdeburg, Universitätsplatz 2, 39106 Magdeburg, Germany*
[b] *Department of Neuroradiology, University Hospital of Magdeburg, Leipziger Straße 44, 39120 Magdeburg, Germany*

Abstract

Background: Radiofrequency ablation was introduced recently to treat spinal metastases, which are among the most common metastases. These minimally-invasive interventions are most often image-guided by flat-panel CT scans, withholding soft tissue contrast like MR imaging. Image fusion of diagnostic MR and operative CT images could provide important and useful information during interventions.

Method: Diagnostic MR and interventional flat-panel CT scans of 19 patients, who underwent radiofrequency ablations of spinal metastases were obtained. Our presented approach piecewise rigidly registers single vertebrae using normalized gradient fields and embeds them within a fused image. Registration accuracy was determined via Euclidean distances between corresponding landmark pairs of ground truth data.

Results: Our method resulted in an average registration error of 2.35 mm. An optimal image fusion performed by landmark registrations achieved an average registration error of 1.70 mm. Additionally, intra- and inter-reader

*Corresponding author
Email address: georg.hille@ovgu.de (Georg Hille)

variability was determined, resulting in mean distances of corresponding landmark pairs of 1.05 mm (MRI) and 1.03 mm (flat-panel CT) for the intra-reader variability and 1.36 mm and 1.28 mm for the inter-reader variability, respectively.

Conclusions: Our multi-segmental approach with normalized gradient fields as image similarity measure can handle spine deformations due to patient positioning and avoid time-consuming manually performed registration. Thus, our method can provide practical and applicable intervention support without significantly delaying the clinical workflow or additional workload.

Keywords: Multi-segmental Image Fusion, Spine Intervention, Interventional Imaging, Normalized Gradient Fields, Automatic Image Registration

---

1. Introduction

Due to the improvement of medical treatment and diagnostic procedures, life expectancy has steadily increased over the last decades. However, this lifetime gain promotes also age-related diseases like cardiovascular diseases, as well as cancer and cancer induced malicious metastases. Beside liver and lungs, bone metastases are the third most likely. Up to two thirds of the latter are located in the spine [1, 2]. Spinal metastases could tremendously affect the quality of life by evoking vigorous pain by fractures, bruises, spinal cord and nerve root compressions or neurologic deficits [3]. Currently, the method of choice to treat painful vertebral metastases is external-beam radiation [4]. However, percutaneous minimally invasive therapies gain increasing reception as a promising alternative. Radio-frequency ablation (RFA) has been used to reduce lower back pain caused by facet osteoarithritis [5]

or osteoid osteoma [6] and was introduced more recently to treat osseous spinal metastases [7].

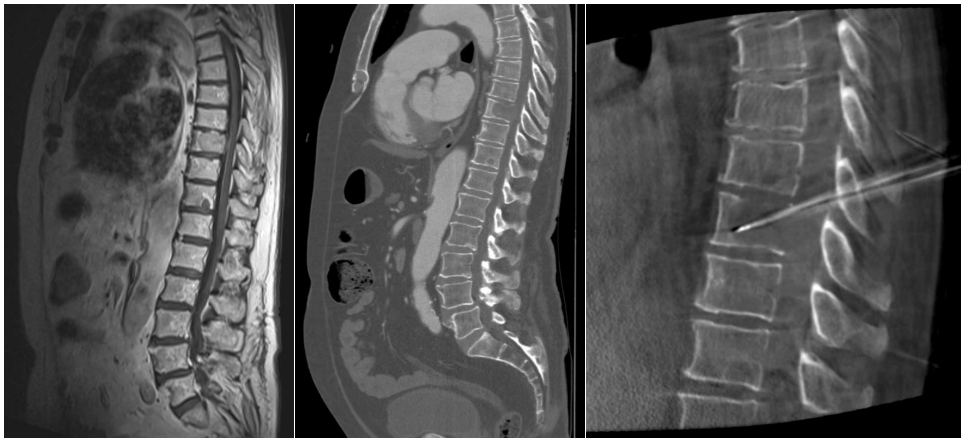

Figure 1: Image modalities that have been used for image-guided interventions of spinal metastases. Sagittal and axial T_1-weighted, T_2-weighted and T_1-weighted contrast-enhanced (left) MR imaging sequences, as well as CT scans (middle) were acquired pre-interventionally. During interventions, flat-panel CT scans (right) support navigation and applicator placement. Artifacts due to low dose protocols, e.g. beam-hardening at the vertebral rim and from inserted metallic instruments aggravate precise metastasis localisation and puncture.

Flat-panel CT and CT angiography are the most common imaging methods regarding image guidance during osseous RF ablations [8, 9, 10]. However, low dose protocols like intra-interventional Dyna-CT scans provide a reduced image quality compared to native CT or MR imaging and weak soft tissue contrast (see Fig. 1). Additionally, it manifests in decreased signal-to-noise ratio (SNR), beam-hardening and scatter artifacts, which hamper precise and reliable metastasis localisation during interventions. Due to the poor visibility of the spinal metastases during interventions, the radiologists have to infer their location from pre-interventionally acquired MRI data and

mentally match those images with the intra-interventionally performed flat-panel CT scans. Thus, a precise localisation is only possible to a certain degree of accuracy. Moreover, each interventional image during the RFA is acquired in prone patient position, causing intervertebral joint movements and altered spine flexion compared to the diagnostic images. This aspect further increases the cognitive load of the radiologists for metastasis puncture, particularly if several metastases are treated in a single procedure [11, 12]. These limitations could be overcome by fusing diagnostic MR images with the intra-interventional scans in order to benefit from the typical MR high soft tissue contrast during interventions. Furthermore, additional image information generated during intervention planning, e.g. segmented metastases or optimized RFA applicator trajectories [13, 14], can be displayed in the interventional images (see Figure 2).

Some studies have been presented regarding image fusion of spine MR and CT imaging. Most of them used landmark-based rigid registration approaches [15, 16, 17, 18]. Alternatively, rigid image fusion could be formulated as an optimisation problem using image similarity measures like mutual information (MI) [19, 20, 21] or normalized gradient fields (NGF) [22, 23]. MI is seen as one of the most suitable similarity measures for multimodal image registration, however, images with sparse structural information, like low dose protocols of interventional flat-panel CT imaging, could yield problems with MI [24]. The most common limitations in fusion of diagnostic spinal MR and interventional flat-panel CT images are differences in patient positioning causing intervertebral joint movements and deformations of the spine structure. Globally rigid techniques like [15, 19] cannot take this into account, therefore, piecewise rigid registration methods with previously segmented vertebral structures or defined region of interests

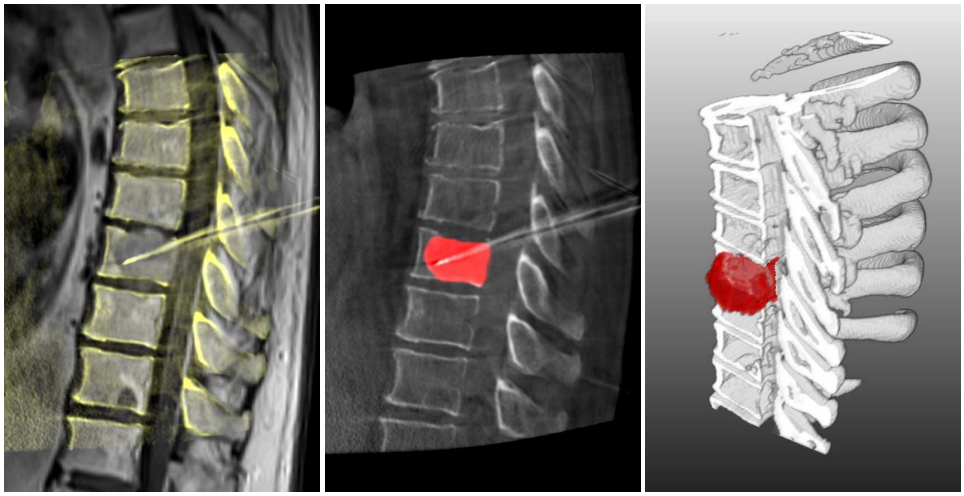

Figure 2: Fusion of pre- and intra-operative images could become a significant improvement of the intervention routine. As a result of the image registration (left; background: MRI, overlay: Dyna-CT) a transformation matrix could be used to transfer and display pre-interventionally produced information like contoured metastases within the intra-interventional images (middle, right).

(ROI) have been reported [16, 17, 21], partly with local rigidity embedded within a global deformation field [20].

Our work combines a multi-segmental registration approach with NGF as an image similarity measure, to cope with deformations of spine structures during RFA interventions of multiple metastases and to overcome limitations of reduced structural information due to low dose interventional imaging. For efficient and convenient applicability within the clinical workflow, the total procedure should not exceed 5 min and should require only minimal user interaction to be performed between the calibration of the navigation system and the metastasis puncture. The mean registration error should be less than 3 mm for being sufficiently precise to likewise enable applicator pathways through vertebral pedicles with mean diameters ranging from 3 to

10 mm (thoracic to lumbar) [25].

2. Materials and Method

2.1. Image data

19 patients who underwent RF ablations of both, single or multiple vertebral metastases, were chosen retrospectively. For diagnostic purposes spine MR imaging was performed pre-interventionally, containing sagittal and axial native T_1- and T_2-weighted sequences, as well as a sagittal STIR (short tau inversion recovery) sequence to enhance oedemata typical due to cancerous and metastatic processes. If required, additional contrast-enhanced T_1-weighted sequences were performed. During the RFA intervention, flat-panel CT scans were acquired to calibrate the navigation system and to validate the final applicator position. We assembled an evalutation set consisting of sagittal native T_1-weighted or contrast-enhanced T_1-weighted MRI sequences and intra-interventionally acquired Dyna-CT scans of each patient. Additionally, we tested the influence of T_2-weighted sequences on our registration approach for five randomly chosen patients. The in-plane image resolution of the MRI data ranged from 0.47 mm to 1.25 mm (average 0.63 mm) and the slice spacing was 3.30 mm for all scans. The flat-panel CT scan resolution ranged from 0.22 mm to 1.10 mm (average 0.65 mm) in-plane and had a slice spacing ranging from 0.46 mm to 3.00 mm (average 1.28 mm). Additionally, segmentation of metastases was performed manually and was for demonstration purposes only (see Figure 2).

2.2. Image Registration

The presented registration approach was selected due to both the physical characteristics of the spine and the available multimodal images. In

our main case of application, in which most patients were in advanced tumor stages and had several vertebral metastases, the intervention region was not limited to a single vertebra, but covered entire spinal segments. A multi-segmental, i.e., piecewise rigid registration procedure appeared to be the most suitable approach in order to accurately model the deformation of spine structures, caused by different patient positioning. Therefore, a global non-rigid image fusion problem was split into multiple local rigid registrations of individual vertebrae or spine segments. To initialize our method, the user had to mark each vertebra or spine segment which has to be registered in both modalities. Following this, regions cropped to single vertebrae or segments were transformed so that their centres coincided in the coordinate origin, taking into account the patient orientation and voxel spacing specified in the DICOM header. This lead to a coarse initial image registration. The anteroposterior length l of those regions was 10 cm, the laterolateral width equaled the MRI volume. Depending on the distance between each marker, we chose the craniocaudal height h. Each ROI is aligned parallel to the vertebral end-plates by rotating it by the orthogonal angle of the connecting line of two marker points.

Subsequently, a three level multi-resolution image-based rigid registration approach precisely registers each ROI with the interventional image combining normalized gradient fields (NGF) [22] as image similarity measure and a Quasi-Newton optimizer. Starting with a rather coarse image resolution, we refined the transformation subsequently on images of increasing resolution until full resolution was reached (downsampling factor was 0.63). NGF are based on a pointwise (continuous) or voxel-based (discrete) distance measure D of the angle between two image gradients, which is defined as

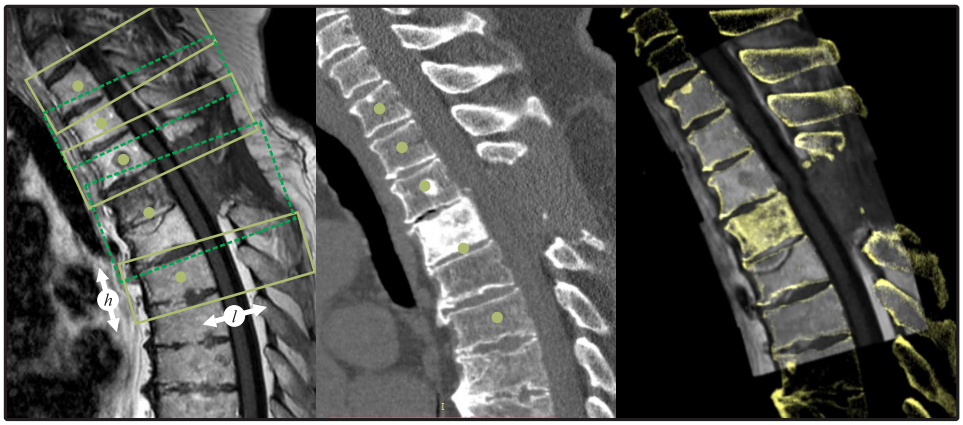

Figure 3: In both imaging modalities the user roughly marks the center (green points) of each region which has to be registered. Subsequently, 3D-ROIs (green contours) are defined and initially translated onto the interventional flat-panel CT image. Our multi-segmental registration approach then precisely and piecewise registers each ROI and embeds them in a fused image (right).

$$\mathcal{D}(A,B) = \frac{1}{2}\int_{\Omega} d(x_A, x_B)dx; \quad d(A,B) = ||v(A,x) \times v(B,x)||^2 \qquad (1)$$

with two corresponding spatial coordinates x in reference image A and template image B, as well as their related gradient vectors $v(A,x)$ and $v(B,x)$ in the image domain Ω. Both vectors form an angle $\theta(x)$ and since the gradient fields are normalized, the cross-product of both vectors is related to the sine of $\theta(x)$. To find a reasonable image registration, the objective function

$$\mathcal{D}(A, B(t)) =: \mathcal{D} \rightarrow min, \qquad (2)$$

has to be minimized, for instance by minimizing the square of the sine of $\theta(x)$. Since NGF are computed by solely taking derivatives into account,

it is well suited for multimodal image registration. The transformed image $B(t) := B \circ t$ is mapped onto the reference image A by a rigid transformation t. Therefore, each transformation T of MR image ROIs to the flat-panel CT scans results from the initial translation I_{tr} multiplied by the image-based registration t, thus $T = t \cdot I_{tr}$. Fusing all transformed and labelled ROIs as well as embedding them in a joint image was the last step in our procedure. Image intensities of voxels with more than one label, e.g., within the area of two overlapping ROIs, were weighted depending on their distance to the specific ROI centres:

$$I_x = \sum_{k=1}^{2} s(1 - d_{xk}) \quad with \quad s(d) = \frac{1}{1 + e^{-20(d-0.5)}}, \tag{3}$$

where d_{xk} represent the relative distances between each voxel x of an overlapping area and the nearest two centres of the transformed ROIs with $\sum d_{xk} = 1$, weighted by a distance-based sigmoid function.

2.3. Evaluation

We carried out experiments with image data of 19 patients who underwent RFA interventions of spinal metastases, treated at the Department of Neuroradiology, Otto-von-Guericke University Hospital Magdeburg, Germany. For each patient, ground truth landmarks were given in both, the diagnostic MRI and the intra-interventionally acquired flat-panel CT images. Three landmarks were determined per vertebra within the sagittal plane of symmetry and on the vertebral rim (superior-anterior, superior-posterior and inferior-posterior corner). The number of labeled vertebra per patient depended on the field of view (FOV) of the flat-panel CT images. The ground truth data of all patients was prepared by a field expert

trained by neuroradiologists. To evaluate registration quality, we determined the mean fiducial registration error (FRE) via averaging Euclidean distance errors between N pairs of corresponding landmarks (transformed MRI landmark $T(p)$ and the flat-panel CT landmark q).

$$FRE = \sqrt{\frac{1}{N}\sum_{i=1}^{N}(T(p_i) - q_i)^2} \tag{4}$$

This was done for the multi-segmental approach, as well as for a global rigid MR image transformation with the same settings, in order to verify the need for a multi-rigid approach to meet clinical accuracy requirements. Registering both landmark sets of each patient directly via Horn's quaternion-based method [26] resulted in a minimal Fiducial Registration Error (mFRE). The mean mFRE represents the error of an optimal global registration of corresponding landmark sets or images. Furthermore, to check inter-reader variability of the ground truth landmark placement, two additional field experts provided ground truth for five randomly chosen patients out of the original 19 cases. Additionally, the first reader created a second ground truth of the same five patients 24 h after the first ground truth preparation to check intra-reader variability without memory bias.

3. Results

The multi-segmental registration of individual vertebrae resulted in average FREs of 2.35 mm and 2.55 mm for fusing intra-interventional Dyna-CT data with diagnostic T_1-weighted and T_2-weighted MR images, respectively. Global rigid registrations of both image datasets resulted in FREs of 3.79 mm (using T_1-weighted MRI data) and 3.87 mm (using T_2-weighted MRI data).

If each patient's corresponding landmark sets were directly registered via Horn's quaternion-based method, a mean mFRE of 1.70 mm was achieved.

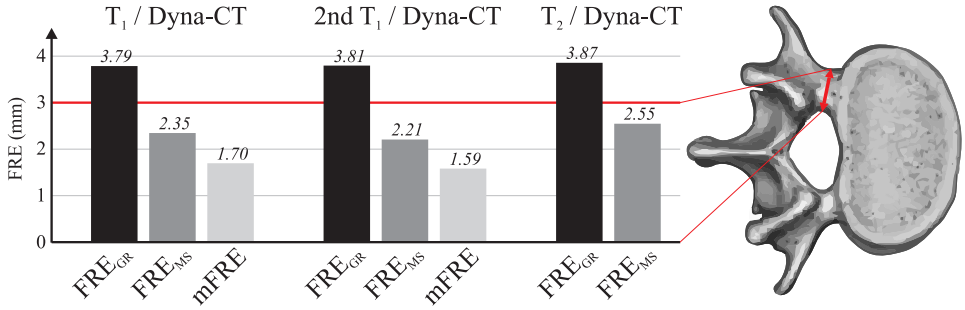

Figure 4: Resulting average registration accuracies of both global rigid image transformations (FRE_{GR}) and the presented multi-segmental approach (FRE_{MS}). We tested image fusion of interventional Dyna-CT images with T_1-, as well as T_2-weighted MR images. Furthermore, to check intra-reader variability, a second ground-truth (2nd T_1) was provided. The red line (at 3 mm) represents the minimum clinical accuracy requirement derived from the mean pedicle diameter [25].

Additionally, intra- and inter-reader variability was checked, resulting in FREs of 1.05 mm (MRI landmarks) and 1.03 mm (Dyna-CT landmarks) for the intra-reader variability and 1.36 mm and 1.28 mm for the inter-reader variability, respectively. The computational time of the registration per vertebra was in average 24 s and the overall required time per patient, including initialization, did not exceed 5 min for any patient. Hence, the requirements of the clinical workflow were met.

4. Discussion

Image fusion has been successfully employed in radiation therapy for the purpose of delineation and enhancement of target fields [27] or to support image-guided interventions [17, 28, 29]. However, in musculoskeletal radiol-

Table 1: Intra- and inter-reader variability were determined for the ground truth data of the MR and the Dyna-CT images. For the intra-reader variability a trained expert provided two ground truth data sets 24 hours apart. The inter-reader variability resulted from matching ground truth data of all three readers with each other and subsequently averaging them.

	MRI	Dyna-CT
FRE_{intra} [mm]	1.05	1.03
FRE_{inter} [mm]	1.36	1.28

ogy, especially in neuroradiology of the spine, image fusion has rarely been reported [15, 16, 20, 21]. For an efficient support of image-guided interventions of spinal metastases, image fusion of diagnostically acquired MR images and interventional flat-panel CT scans plays an important role. MR imaging is considered the method of choice regarding tumour and metastasis delineation as well as for information about compression of spinal nerve roots and the spinal canal, due to its emphasised soft tissue contrast. Though, RFAs are performed under flat-panel CT image guidance, which mainly withholds relevant image information. Therefore, fusion of both image modalities could provide various additional information to support applicator placement and treatment verification beyond the established methods of current navigation systems [10, 30].

In our study, we have evaluated a multi-segmental image-based registration approach to combine diagnostic MR and interventional flat-panel CT images. Table 2 displays an overview of relevant information about the presented and related work, though some of the latter did not state any

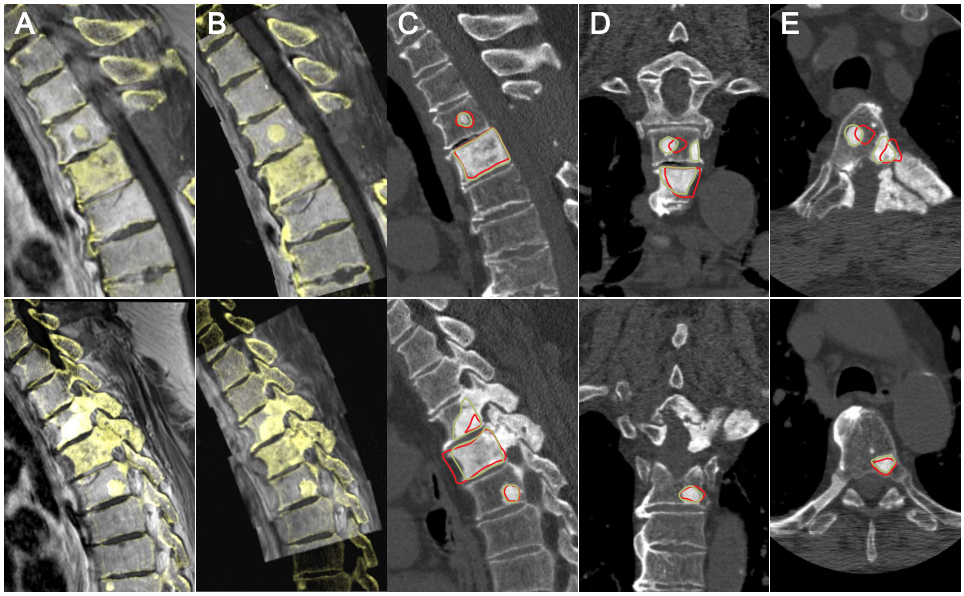

Figure 5: Comparison between a global rigid (A) and our multi-segmental (B) registration approach in a mid-sagittal (top row) and lateral (bottom row) cross-section. Additionaly, the masks of previously segmented metastases were transformed according to the resulting transformation matrices of both methods (C - E). The global rigid method (red) proved not to be sufficiently accurate with a mean FRE_{GR} of 4.58 mm for this case, while our approach (green) meets the clinical accuracy requirements with a mean FRE_{MS} of 1.84 mm.

quantitative results, which restricts comparability. In contrast to the related work of spinal image fusion, we focused on interventional rather than diagnostic CT imaging. Thus, we had to deal with qualitatively inferior images, due to the low-dose protocols during interventions. So far, either landmark-based approaches [15, 16, 17] or mutual information as a registration metric [19, 20, 21] have been used. The former usually have the disadvantage of a time consuming initialization procedure, which grows proportionally with the number of landmarks. The study of Kaminsky et al. [16], for instance, required over 8 min per vertebra (vs. our average 24 s),

which proves to be impracticable in terms of intervention support. Likewise, a preceding vertebrae segmentation to define the regions to be registered, as presented by [20, 21, 31], is time-consuming and the question arises what effects inaccurate segmentations will have on the registration accuracy. Hu et al. [21] reported an overall time required of approximately 60 min, which is hardly compatible with clinical procedures. Our method, however, only requires an approximate marking of the vertebrae to be registered, which reduces the required time for initialisation as well as the cognitive load of radiologists and can therefore, be easily integrated into the clinical workflow. Furthermore, NGF proved superior to MI as a registration metric (average FRE_{MS} of 2.35 mm versus 2.87 mm). The interventional CT images showed less soft tissue contrast, often only the vertebral rim was displayed compared to native CT scans, which is why a gradient based metric performed better. To compensate spine deformations caused by different patient positioning between diagnostic and interventional imaging, we chose a multi-segmental approach, since the global rigid transformations' accuracy often proved to be insufficiently. Thus, the average FRE_{MS} with 2.35 mm was significantly more precise than the average FRE_{GR} with 3.82 mm (see Fig. 5). Overall, our presented method met the clinical accuracy requirements of a maximum permissible registration error of 3 mm.

Slightly higher FREs have been observed when using T_2- instead of T_1-weighted MR images. This could partly be attributed to the somewhat better contrast of the T_1 images at the transition between the dorsal vertebral rim and spinal canal, which suits the gradient-based registration metric. The mFRE with 1.70 mm represented the mean deviation of an optimal global rigid registration of both landmark sets. Inaccuracies during landmark placing, high slice spacing of the MRI data, as well as spine structure deforma-

Table 2: Related and the presented work in comparison. MR/CT - diagnostical imaging, FP-CT - interventional flat-panel CT imaging, Interv. - interventional Images, MI - mutual information, LMB - landmark-based, NGF - normalized gradient fields, Transform. - transformation type, FRE - fiducial registration error, t - average time required per dataset, t^* - average time required per vertebra, n.s. - not stated

Works	Image Data	N_P	Interv.	Metric	Transform.	FRE [mm]	t
Hu [21]	MR / CT	1	-	MI	multi-rigid	n.s.	> 60 min
Kaminsky [16]	MR / CT	1	-	LMB	multi-rigid	1.53	> 8 min*
Čech [20]	MR / CT	3	-	MI	multi-rigid	n.s.	n.s.
Sohn [17]	MR / CT	20	-	LMB	global rigid	n.s.	n.s.
Karlo [15]	MR / CT	10	-	LMB	global rigid	1.46	~ 2 min
Miles [19]	MR / CT	20	-	MI	global rigid	1.90	n.s.
Ours	MR/FP-CT	19	+	NGF	multi-rigid	2.35	24 s*

tions due to patient positioning contribute to this error. Furthermore, we investigated intra- and inter-reader variability. As expected, average intra-reader variability was significantly lower than inter-reader variability, since various readers interpret the given guidelines slightly different. Even though, the anatomical landmark positions were clearly defined in theory, inaccuracies occurred, because the vertebral rim was several voxels wide and the sagittal plane of symmetry was difficult to determine accurately and reproducibly. The intra- and inter-reader variability of landmarks placed in the MR images were slightly higher than those in the Dyna-CT, which is due to the lower MR spatial resolution.

5. Conclusion

In this work, we presented an applicable and precise registration approach to fuse diagnostical MR and interventional flat-panel CT images for the purpose of intervention support. It is the only method to date, which combines an image-based and multi-segmental approach and takes interventional image data into account. The choice of the image fusion method was determined by both physical characteristics of the spine as well as the requirements and the workflow during RFA interventions of spinal metastases. A multi-segmental approach with NGF as an image similarity measure seemed to be the most suitable to model spine deformations due to patient positioning and to avoid the time-consuming initialization of a landmark-based registration. This enables our method to provide practical and applicable intervention support without significantly delaying the clinical workflow or being too much additional workload. In future work, we would like to integrate our application into a comprehensive workflow support for RF ablations of spinal metastases, e.g. by including an automatically performed metastasis detection [32] with a subsequent segmentation step, either manual or semi-automatic, as part of the intervention planning and prior to the presented registration approach.

Ethical approval: All procedures performed in studies involving human participants were in accordance with the ethical standards of the institutional and/or national research committee and with the 1964 Helsinki declaration and its later amendments or comparable ethical standards. For this type of study formal consent is not required.

Funding: This work was funded by the Federal Ministry of Education and Research within the Forschungscampus *STIMULATE* (grant number 13GW0095A).

Conflict of Interest Statement: None declared.

References

[1] K. Harrington, Metastatic disease of the spine, Journal of Bone and Joint Surgery 68 (7) (1986) 1110–1115.

[2] D. A. Wong, V. L. Fornasier, I. MacNab, Spinal metastases: the obvious, the occult, and the impostors, Spine 15 (1990) 1–4.

[3] P. Klimo, M. H. Schmidt, Surgical management of spinal metastases, The Oncologist 9 (2) (2004) 188–196.

[4] S. Lutz, L. Berk, E. Chang, E. Chow, C. Hahn, P. Hoskin, D. Howell, A. Konski, L. Kachnic, S. Lo, et al., Palliative radiotherapy for bone metastases: an astro evidence-based guideline, International Journal of Radiation Oncology Biology Physics 79 (2011) 965–976.

[5] J. Cho, Y. G. Park, S. S. Chung, Percutaneous radiofrequency lumbar facet rhizotomy in mechanical low back pain syndrome, Stereotactic and functional neurosurgery 68 (1997) 212–217.

[6] D. I. Rosenthal, F. J. Hornicek, M. W. Wolfe, L. C. Jennings, M. C. Gebhardt, H. J. Mankin, Percutaneous radiofrequency coagulation of osteoid osteoma compared with operative treatment, J Bone Joint Surg Am 80 (1998) 815–21.

[7] D. E. Dupuy, D. Liu, D. Hartfeil, L. Hanna, J. D. Blume, K. Ahrar, R. Lopez, H. Safran, T. DiPetrillo, Percutaneous radiofrequency ablation of painful osseous metastases, Cancer 116 (2010) 989–997.

[8] A. Posteraro, D. Dupuy, W. Mayo-Smith, Radiofrequency ablation of bony metastatic disease, Clinical radiology 59 (9) (2004) 803–811.

[9] J. Palussiere, A. Pellerin-Guignard, E. Descat, F. Cornélis, F. Dixmérias, Radiofrequency ablation of bone tumours, Diagnostic and interventional imaging 93 (9) (2012) 680–684.

[10] P. Kavakebi, C. Freyschlag, C. Thomé, How I do it: optimizing radiofrequency ablation in spinal metastases using iCT and navigation, Acta Neurochirurgica 159 (10) (2017) 2025–2028.

[11] A. Wallace, A. Tomasian, D. Vaswani, R. Vyhmeister, R. Chang, J. Jennings, Radiographic local control of spinal metastases with percutaneous radiofrequency ablation and vertebral augmentation, American Journal of Neuroradiology 37 (4) (2016) 759–765.

[12] T. J. Greenwood, A. Wallace, M. V. Friedman, T. J. Hillen, C. G. Robinson, J. W. Jennings, Combined ablation and radiation therapy of spinal metastases: a novel multimodality treatment approach, Pain Physician 18 (6) (2015) 573–581.

[13] C. Baegert, C. Villard, P. Schreck, L. Soler, A. Gangi, Trajectory optimization for the planning of percutaneous radiofrequency ablation of hepatic tumors, Computer Aided Surgery 12 (2) (2007) 82–90.

[14] A. Seitel, M. Engel, C. M. Sommer, B. A. Radeleff, C. Essert-Villard, C. Baegert, M. Fangerau, K. H. Fritzsche, K. Yung, H.-P. Meinzer, et al., Computer-assisted trajectory planning for percutaneous needle insertions, Medical physics 38 (6Part1) (2011) 3246–3259.

[15] C. Karlo, I. Steurer-Dober, M. Leonardi, C. Pfirrmann, M. Zanetti, J. Hodler, MR/CT image fusion of the spine after spondylodesis: a feasibility study, European Spine Journal 19 (10) (2010) 1771–1775.

[16] J. Kaminsky, T. Rodt, J. Zajaczek, F. Donnerstag, M. Zumkeller, Mehrsegmentale Bildfusion an der Wirbelsäule/Multisegmental Image Fusion of the Spine, Biomedical Engineering 49 (3) (2004) 49–55.

[17] M.-J. Sohn, D.-J. Lee, S. W. Yoon, H. R. Lee, Y. J. Hwang, The effective application of segmental image fusion in spinal radiosurgery for improved targeting of spinal tumours, Acta neurochirurgica 151 (3) (2009) 231–238.

[18] Y.-T. Chen, M.-S. Wang, Three-dimensional reconstruction and fusion for multi-modality spinal images, Computerized Medical Imaging and Graphics 28 (1-2) (2004) 21–31.

[19] B. Miles, I. B. Ayed, M. W. Law, G. Garvin, A. Fenster, S. Li, Spine image fusion via graph cuts, IEEE Transactions on Biomedical Engineering 60 (7) (2013) 1841–1850.

[20] P. Čech, A. Andronache, L. Wang, G. Székely, P. Cattin, Piecewise rigid multimodal spine registration, in: Proc. of Bildverarbeitung für die Medizin, Springer, 2006, pp. 211–215.

[21] Y. Hu, D. R. Haynor, Multirigid registration of MR and CT images of the cervical spine, in: Proc. of Medical Imaging: Image Processing, Vol. 5370, International Society for Optics and Photonics, 2004, pp. 1527–1539.

[22] E. Haber, J. Modersitzki, Intensity gradient based registration and fusion of multi-modal images, in: Proc. of International Conference on Medical Image Computing and Computer-Assisted Intervention (MICCAI), Springer, 2006, pp. 726–733.

[23] F. Tramnitzke, J. Rühaak, L. König, J. Modersitzki, H. Köstler, Gpu based affine linear image registration using normalized gradient fields, in: Proc. of Seventh International Workshop on High Performance Computing for Biomedical Image Analysis (HPC-MICCAI), 2014.

[24] A. Andronache, P. Cattin, G. Székely, Adaptive subdivision for hierarchical non-rigid registration of multi-modal images using mutual information, in: International Conference on Medical Image Computing and Computer-Assisted Intervention (MICCAI), Springer, 2005, pp. 976–983.

[25] P. V. Scoles, A. E. Linton, B. Latimer, M. E. Levy, B. F. Digiovanni, Vertebral body and posterior element morphology: the normal spine in middle life, Spine 13 (10) (1988) 1082–1086.

[26] B. K. Horn, Closed-form solution of absolute orientation using unit quaternions, JOSA A 4 (4) (1987) 629–642.

[27] E. Z. Dalah, A. Nisbet, S. Reise, D. Bradley, Evaluating commercial image registration packages for radiotherapy treatment planning, Applied Radiation and Isotopes 66 (12) (2008) 1948–1953.

[28] S. F. Nemec, M. A. Donat, S. Mehrain, K. Friedrich, C. Krestan, C. Matula, H. Imhof, C. Czerny, CT–MR image data fusion for computer assisted navigated neurosurgery of temporal bone tumors, European Journal of Radiology 62 (2) (2007) 192–198.

[29] G. Mauri, L. Cova, S. De Beni, T. Ierace, T. Tondolo, A. Cerri, S. N. Goldberg, L. Solbiati, Real-time us-ct/mri image fusion for guidance of thermal ablation of liver tumors undetectable with us: results in 295 cases, Cardiovascular and interventional radiology 38 (1) (2015) 143–151.

[30] D. Wallach, G. Toporek, S. Weber, R. Bale, G. Widmann, Comparison of freehand-navigated and aiming device-navigated targeting of liver lesions, The International Journal of Medical Robotics and Computer Assisted Surgery 10 (1) (2014) 35–43.

[31] G. Hille, S. Saalfeld, S. Serowy, K. Tönnies, Vertebral body segmentation in wide range clinical routine spine mri data, Computer Methods and Programs in Biomedicine 155 (2018) 93–99.

[32] J. Wang, Z. Fang, N. Lang, H. Yuan, M.-Y. Su, P. Baldi, A multiresolution approach for spinal metastasis detection using deep

siamese neural networks, Computers in Biology and Medicine 84 (2017) 137–146.